Through-Space Conjugation: An Effective Strategy for Stabilizing Intramolecular Charge-Transfer States

Pingchuan Shen,[†] Zeyan Zhuang,[†] Xiao-Fang Jiang,[†] Jinshi Li,[†] Shunan Yao,[†] Zujin Zhao,*,[†] and Ben Zhong Tang*,[†,‡]

[†]State Key Laboratory of Luminescent Materials and Devices, Center for Aggregation-Induced Emission, South China University of Technology, Guangzhou 510640, China

[‡]Department of Chemistry, Hong Kong Branch of Chinese National Engineering Research Center for Tissue Restoration and Reconstruction, The Hong Kong University of Science & Technology, Clear Water Bay, Kowloon, Hong Kong, China

S *Supporting Information*

ABSTRACT: Intramolecular charge transfer (ICT) has significant impacts on organic optoelectronic materials, photochemistry, biotechnology, and so on. However, it is hard to stabilize the ICT state because of the rapid nonradiative charge recombination process, which often quenches light emission. In this work, we use new foldamers of the protonated pyridine-modified tetraphenylethene derivatives that possess through-space conjugation (TSC) characters as the models to study the impact of TSC on the ICT state. Steady and transient spectroscopies illustrate that the lifetime of the ICT state in the molecule with strong TSC can be much longer than those of molecules without TSC, giving rise to a higher fluorescence quantum yield. By combining the theoretical calculations, we demonstrate that the strong TSC can stabilize the ICT state and slow the charge recombination rate by more efficiently dispersing charges. This is a conceptually new design strategy for functional optoelectronic materials that require more stable ICT states.
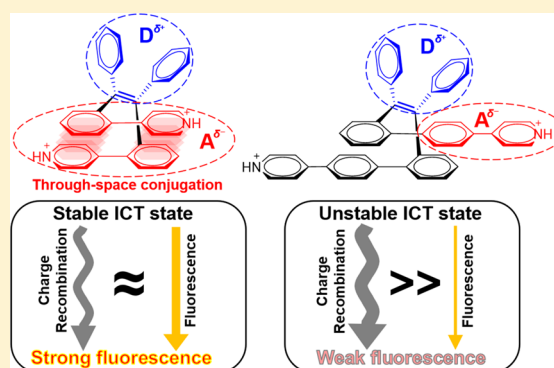
The in-depth understanding of the intramolecular charge transfer (ICT) state is of high importance for the development of organic optoelectronic materials.[1−3] For example, in artificial photosynthesis, the efficient use of sunlight requires the suitable photogenerated ICT states to yield applicable photocurrent.[4,5] For dye-sensitized organic solar cells, the ICT state can provide the driving force of the electron transfer.[6] Molecules with electronic donor−acceptor (D−A) structures are widely used for ICT study. When D−A molecules are excited by photonic or electronic energies, a charge separation process occurs, which leads to a transient ICT state that quickly decays through radiative transitions and much faster nonradiative manners such as a charge recombination process. Therefore, the lifetime of the ICT state is very short, which greatly limits the optoelectronic performance in certain areas.[7] Generally, short and well-conjugated bridges can help to increase the rate of the charge separation process and facilitate charge migration,[8,9] but the resulting stronger D−A interactions will accelerate the charge recombination process and shorten the lifetime of the ICT state. Hence, for the D−A molecules, it seems difficult to achieve fast charge transport and a long-lived ICT state at the same time.

Recently, certain π-stacked aromatic systems with unique through-space conjugation (TSC) have drawn much attention, in which the electron cloud can delocalize in the inter-ring regions of closely face-to-face aligned aromatic rings.[10,11] Diverse TSC systems based on cyclophane,[12−16] naphthalene,[17−19] hexaarylbenzene,[20−22] xanthene,[23,24] helical foldamers,[25−27] self-assembled cages,[28,29] metal−organic frameworks,[30] etc.[31,32] have been reported to have prominent capacity of transporting charge and energy via a spatial channel. In our previous works, we developed a series of novel through-space conjugated foldamers containing a tetraphenylethene (TPE) skeleton,[33−35] which hold distinct advantages such as efficient multidimensional charge and energy transport abilities.[36−38] The previous works indicate that the TSC may be considered as a positive factor for these advantages by stabilizing the ICT state in these foldamers. As a proof of concept, in this work, we design several new TPE-based foldamers bearing pyridine and protonated pyridine to systematically study the impact of TSC on the ICT state. Steady spectroscopy is used to study the ICT properties of these foldamers, and transient optical spectra are obtained to analyze the decay processes and lifetimes of ICT states. In addition, theoretical calculation based on density functional theory and time-dependent density functional theory are carried out to demonstrate the TSC characters in frontier
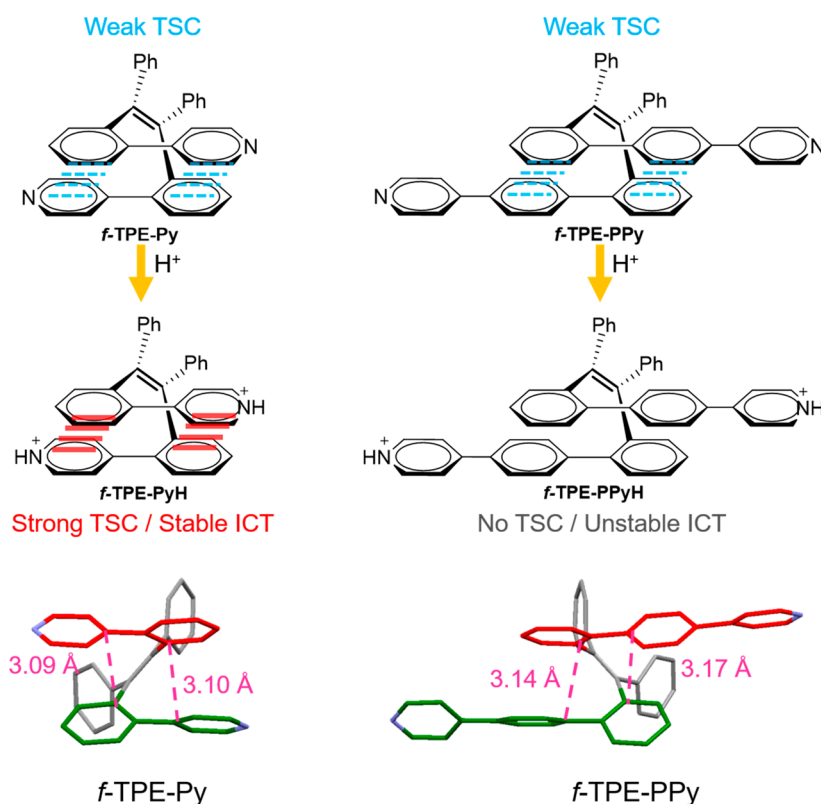
Scheme 1. Molecular Structures of *f*-TPE-Py, *f*-TPE-PPy, *f*-TPE-PyH, and *f*-TPE-PPyH and Crystal Structures of *f*-TPE-Py and *f*-TPE-PPy[a]

[a]TSC, through-space conjugation; ICT, intramolecular charge transfer.

orbitals and their contributions to the transitions. The results reveal that TSC can stabilize the ICT state efficiently, rendering enhanced fluorescence of D−A molecules.

The foldamers *f*-TPE-Py and *f*-TPE-PPy are stereoselectively prepared according to synthetic procedures reported in the literature,[34,37] and their folded structures are also proved by the crystal structures (Scheme 1). It can be seen that the two linear fragments are aligned closely and largely overlapped with short interplane distances of ≤3.17 Å, implying efficient TSC characters.[39] The protonated *f*-TPE-PyH and *f*-TPE-PPyH are obtained in acid solution (pH < 1.78), as disclosed by the absorption spectra titration (Figure S1). Only one isosbestic point is found in the absorption spectra for each *f*-TPE-PyH and *f*-TPE-PPyH, which indicates that two pyridine rings in these foldamers are protonated at the same pH value, and the single-protonated intermediates are hardly found. Photoluminescence (PL) spectra titrations show that the protonation processes of these foldamers are reversible. With the addition of basic solution, the deprotonation process occurs, and the PL spectra recover to the original state (Figure S2). In addition, in the ^{1}H NMR spectra (Figure S3A,B), distinctive peaks at ∼5.7 ppm are observed for both unprotonated and protonated foldamers, which are notably up-shifted compared to the proton peaks in common aromatic molecules. These peaks are attributed to the protons on the π-stacked phenyl rings, which are strongly shielded by ring-current effect of the opposite phenyl ring, as confirmed by our previous works.[34−40] These results reveal that these molecules can maintain folded structures after being protonated.

To understand the influence of TSC on the absorption property, peak differentiating and imitating are conducted on

the experimental absorption spectra under the guide of theoretical calculation (Figure S4). The unprotonated foldamers *f*-TPE-Py and *f*-TPE-PPy exhibit main absorption peaks at 306 and 280 nm, respectively, with long absorption tails extending to ∼390 nm (Figure 1A,B). The maximum absorption peaks of *f*-TPE-Py and *f*-TPE-PPy can be resolved into two peaks. The long-wavelength peaks (∼330 nm) are assigned to the $S_0 \rightarrow S_1$ transitions, which are dominated by the TPE fragment. These absorption bands originate from locally excited (LE) states. The short-wavelength peaks (∼310 nm) are associated with the higher-energy transitions involving the LUMO+1 orbitals that have distinct TSC character and make significant contributions to the absorption (Figure 1E,F).[39] The TSC characters of *f*-TPE-Py and *f*-TPE-PPy are more prominent in the orbitals with high energy levels and have little contribution in $S_0 \rightarrow S_1$ transition, which is extremely crucial for photophysical properties.

However, the protonated foldamers *f*-TPE-PyH and *f*-TPE-PPyH have quite different absorption properties. The main absorption peak of *f*-TPE-PyH is located at 270 nm, with a broad absorption tail extending to ∼420 nm (Figure 1C). The major peak is assigned to the $S_0 \rightarrow S_3$ transition which mainly occurs in the TPE moiety, while the absorption tail is associated with the transitions of $S_0 \rightarrow S_1$ and $S_0 \rightarrow S_2$. The absorption tail exhibits apparent ICT character (Figure 1G). Because the protonated pyridine is a stronger electron acceptor in comparison with pyridine itself, the energy level of the ICT state in *f*-TPE-PyH is much lower than that of the LE state.[41,42] Hence, the absorption tail in *f*-TPE-PyH's spectrum should be attributed to the absorption of the ICT state. More interestingly, the TSC of *f*-TPE-PyH appears in the LUMO
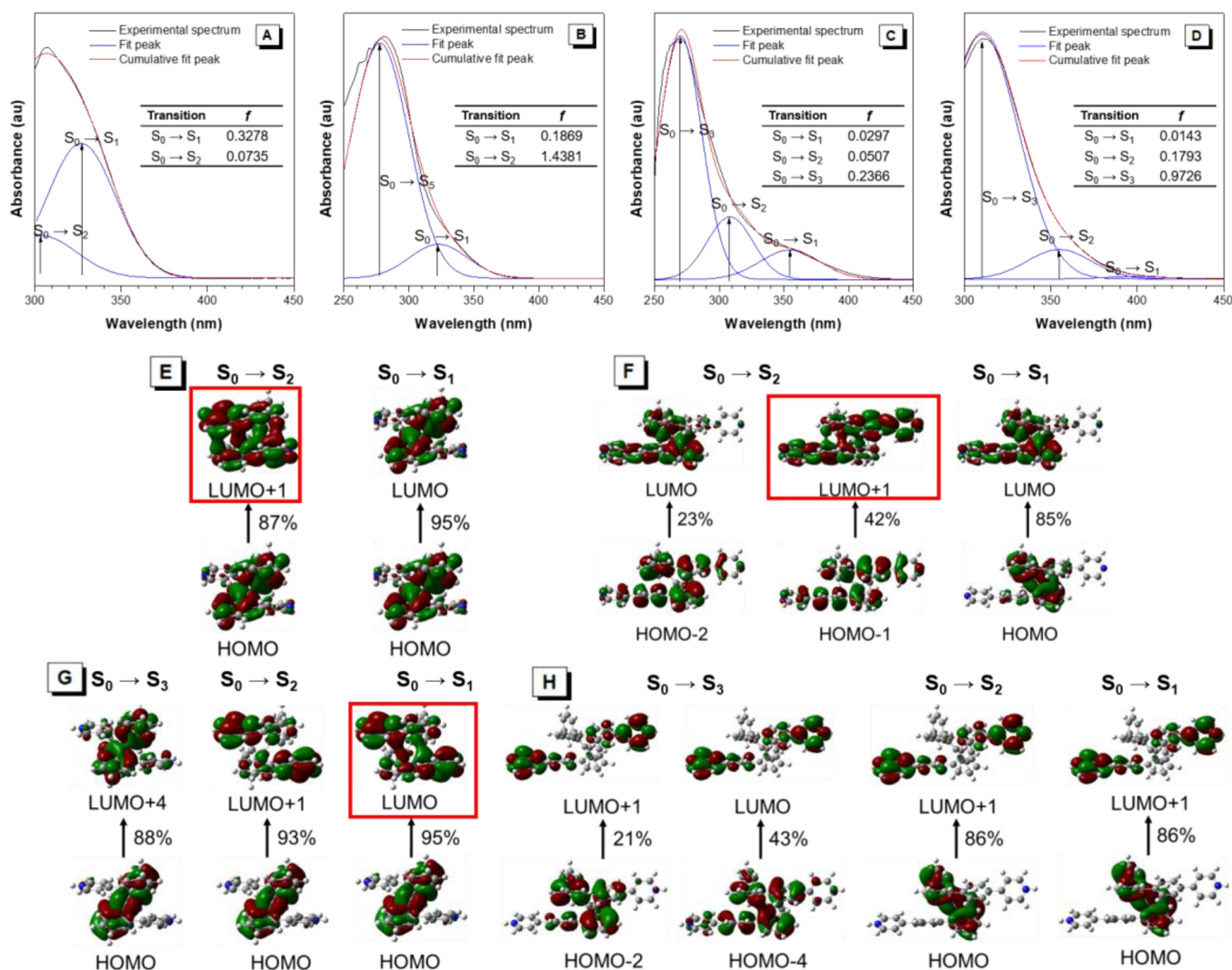
Figure 1. Experimental UV−vis absorption spectra (black) and the peak differentiating (blue) and imitating (red) of (A) *f*-TPE-Py, (B) *f*-TPE-PPy, (C) *f*-TPE-PyH, and (D) *f*-TPE-PPyH. The absorption spectra were measured in 1,4-dioxane. For *f*-TPE-PyH and *f*-TPE-PPyH, the pH of the solution is 1.2. The inserted tables are the calculated oscillator strengths of transitions. Orbital amplitude plots of (E) *f*-TPE-Py, (F) *f*-TPE-PPy, (G) *f*-TPE-PyH, and (H) *f*-TPE-PPyH.

rather than LUMO+1 and makes the largest contribution to $S_0 \rightarrow S_1$ transition. The TSC orbital of *f*-TPE-PyH is located at a lower energy level in comparison with that of *f*-TPE-Py, indicating that the TSC orbital of *f*-TPE-PyH is more stable. Therefore, the TSC of *f*-TPE-PyH is stronger than that of *f*-TPE-Py, which should have a positive effect to disperse the positive charge between the stacked phenyl and protonated pyridine rings. In that case, the energy level of the ICT state is lowered, giving rise to a more extensive absorption tail. The strongest absorption peak of *f*-TPE-PPyH is located at 310 nm, resulting from the high-energy transition of $S_0 \rightarrow S_3$. The extensive absorption tail reaching ~410 nm is related to low-energy transitions of $S_0 \rightarrow S_1$ and $S_0 \rightarrow S_2$, which are clearly red-shifted relative to that of *f*-TPE-PPy because of the ICT effect. However, no apparent character of TSC is found in the frontier orbitals, indicating that TSC disappears in *f*-TPE-PPyH.

The solvatochromism experiment is further employed to investigate the ICT character of the foldamers. According to the Lippert−Mataga equation, the Stokes shift of the chromophores is affected by the solvents' orientation polarity

(Δf).[43] In these experiments, 1,4-dioxane, tetrahydrofuran (THF), *N*,*N*-dimethylformamide (DMF), and acetonitrile (MeCN) with Δf values of 0.021, 0.210, 0.275, and 0.306, respectively, are used.[44] As shown in Figure 2A,B, the PL peaks of the unprotonated foldamers *f*-TPE-Py and *f*-TPE-PPy are located at ~480 nm in 1,4-dioxane and remain almost unchanged as the solvent polarity increases, demonstrating that the PL of *f*-TPE-Py and *f*-TPE-PPy mainly comes from the LE state. Because the electron-withdrawing ability of pyridine groups is relatively weak, the push−pull interaction between TPE core and pyridine is relatively weak as well. In that case, the ICT effect becomes much weak, and the PL from ICT states can hardly be found for *f*-TPE-Py and *f*-TPE-PPy. Nevertheless, the protonated foldamers *f*-TPE-PyH and *f*-TPE-PPyH show remarkable solvatochromic effect because the electron-withdrawing ability of protonated pyridine is greatly enhanced. Taking *f*-TPE-PyH as an example (Figure 2C), its PL peak is located at 526 nm in 1,4-dioxane, while in acetonitrile, the PL peak is red-shifted to 553 nm, indicating that the PL of *f*-TPE-PyH involves ICT state. In addition, the comparison between excitation and absorption spectra (Figure
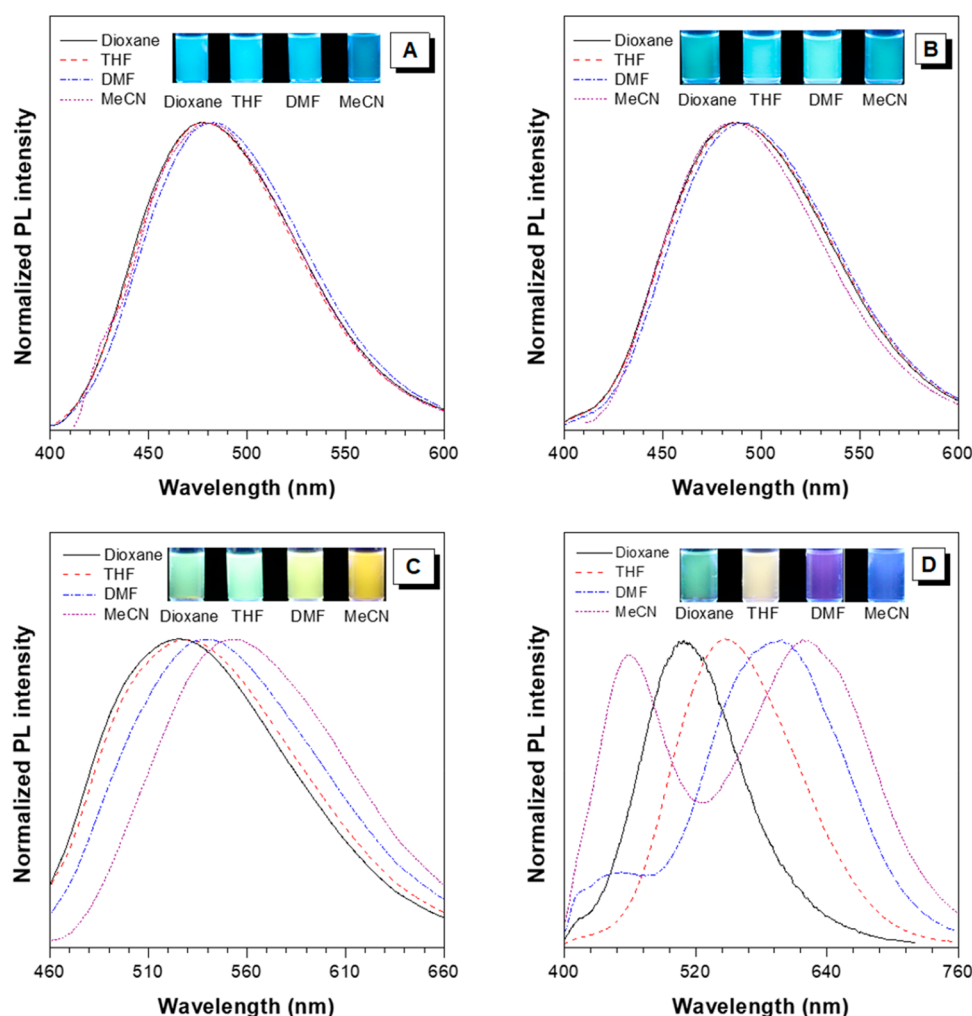
Figure 2. PL spectra of *f*-TPE-Py, *f*-TPE-PPy, *f*-TPE-PyH, and *f*-TPE-PPyH in different solvents. The fluorescent photos are taken under the illumination of a UV lamp (365 nm).

S5A and C) reveals that the excitation bands overlap with the absorption bands of ICT state to a large extent, while the absorption bands that are attributed to the LE state have less overlap with the excitation bands. Considering that the absorption band of ICT state is closely correlated to the orbitals with TSC character in *f*-TPE-PyH, TSC indeed should have exerted significant impact over the PL property of *f*-TPE-PyH. The solvatochromic effect is also found for *f*-TPE-PPyH. However, when the polarity of the solvent increases, not only the red-shifted PL peak but also a new blue PL peak at around 450 nm appears in high polar solvents (Figure 2D). According to the excitation spectra of *f*-TPE-PPyH (Figure S5D), for PL peaks of 450 and 620 nm, the excitation peak is located at 370 nm, which is highly relevant to the absorption band of the ICT state. Thus, it is more possible that the blue PL peak originates from one of the 4-(biphenyl-4-yl)pyridine moieties instead of the TPE moiety. To prove this speculation, a reference molecule of protonated 4-(biphenyl-4-yl)pyridine (PPyH) (Figure S6) is synthesized and studied. PPyH shows deep blue light at 430 nm in acetonitrile, which is close to the blue PL of *f*-TPE-PPyH (450 nm) in acetonitrile. These results demonstrate that the blue PL peak of *f*-TPE-PPyH should stem from the 4-(biphenyl-4-yl)pyridine moiety.

Radiative and nonradiative decay rates (k_r and k_{nr}, respectively) are highly useful to depict the ICT states.

Table S1 lists the k_r and k_{nr} of the four foldamers in different solvents. When solvent polarity increases, the k_r of *f*-TPE-PPyH decreases greatly while the k_{nr} increase greatly. In acetonitrile, the k_{nr} (5.59×10^8 s^{-1}) of *f*-TPE-PPyH is nearly 2 orders of magnitude higher than the k_r (0.06×10^8 s^{-1}). However, for *f*-TPE-PyH, only slightly decreased k_r and k_{nr} are observed when solvent polarity increases. Even in acetonitrile, the k_r (0.17×10^8 s^{-1}) and k_{nr} (0.92×10^8 s^{-1}) of *f*-TPE-PyH are still comparable, indicating that *f*-TPE-PyH should have a different ICT process in comparison with *f*-TPE-PPyH. Similar results can also be observed not only in solutions but also in solid films (Table S2). In solid film, the values of Φ_F, k_r, and k_{nr} of *f*-TPE-Py and *f*-TPE-PPy are comparable. After being protonated, the Φ_F of *f*-TPE-PyH is 20.2%, which is greater than that of *f*-TPE-PPyH (1.1%). The k_r of *f*-TPE-PyH (0.15×10^8 s^{-1}) is much larger than that of *f*-TPE-PPyH (0.02×10^8 s^{-1}), and the k_{nr} of *f*-TPE-PyH (0.59×10^8 s^{-1}) is much smaller than that of *f*-TPE-PPyH (1.62×10^8 s^{-1}). Owing to the shorter distance between D and A groups, *f*-TPE-PyH is supposed to have a stronger D−A interaction and thus has a larger k_{nr} which is dominated by a charge recombination process. However, the fact is that the k_{nr} of *f*-TPE-PyH is apparently reduced relative to that *f*-TPE-PPyH regardless of being in solution or solid film. A reasonable hypothesis is that
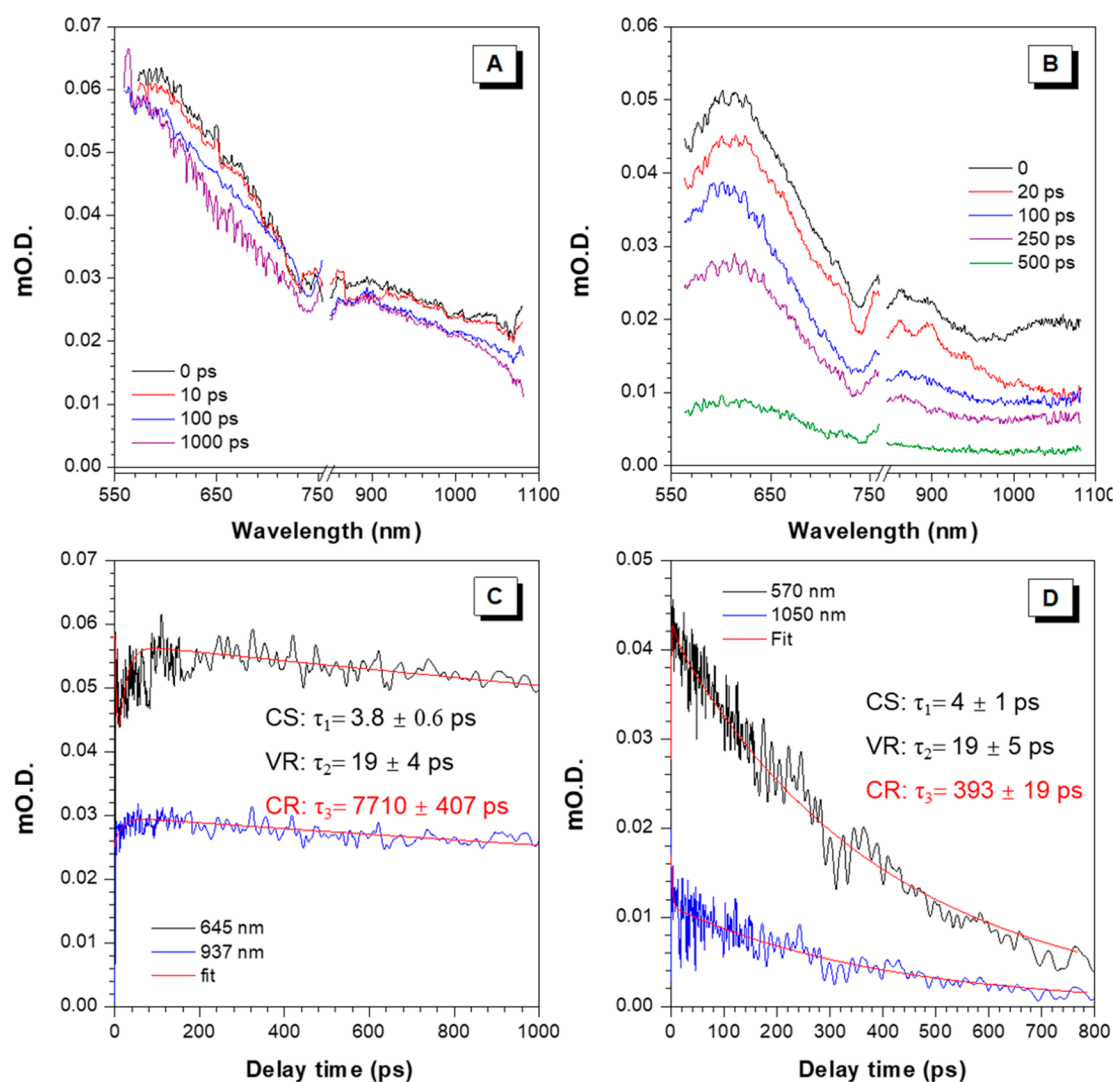
Figure 3. Transient absorption spectra of (A) *f*-TPE-PyH and (B) *f*-TPE-PPyH in acetonitrile, excited at 400 nm. Spectral relaxation for (C) *f*-TPE-PyH and (D) *f*-TPE-PPyH in acetonitrile (10^{-4} M). Theoretically fitted curves are shown as red solid lines. CS, charge separation; VR, vibration relaxation; CR, charge recombination.

the strong TSC of *f*-TPE-PyH stabilizes the charge-separated ICT state, which is conducive to the PL.

To further validate that TSC has the positive effect of stabilizing the ICT state, femtosecond transient absorption (fsTA) spectra are measured to study the excited-state properties of *f*-TPE-PyH and *f*-TPE-PPyH. The photo-excitation at 400 nm with a 50 fs laser pulse is used to produce the ICT states of *f*-TPE-PyH and *f*-TPE-PPyH. To better analyze the excited-state absorption properties, the stimulated radiation signals are filtered through system design, and the excited-state absorption signals are observed in the range of 550−1100 nm (Figure 3). There are two main peaks at 570 and 937 nm for *f*-TPE-PyH, and only slight decay of the peaks is observed in a time scale from 0 to 1000 ps (Figure 3A). However, the excited-state absorption signals of *f*-TPE-PPyH at 570, 875, and 1050 nm decay rapidly to zero within 500 ps.

All the profiles monitored can be expressed by triexponential functions with decay times of 3.8 ± 0.6, 16 ± 2, and 7710 ± 407 ps for *f*-TPE-PyH and 4 ± 1, 18 ± 2, and 393 ± 19 ps for *f*-TPE-PPyH. The first kinetic components (3.8 ± 0.6 and 4 ± 1 ps) of these two molecules should be interpreted as the

charge-separation process.[45] The second kinetic components with tens of picoseconds (16 ± 2 and 18 ± 2 ps) after the charge-separation process are attributed to the vibrational relaxation related with molecular conformation change.[45] Because there are only minor conformational variations between ground and excited states for both molecules, as revealed by the calculation results (Figure S7), the rates of vibration relaxation processes in *f*-TPE-PyH and *f*-TPE-PPyH are very close. The last kinetic components have the longest lifetimes, associated with the charge recombination process. The lifetime of charge recombination process of *f*-TPE-PyH reaches the nanosecond level (∼7.7 ns), which is nearly 20-fold longer than that of *f*-TPE-PPyH (393 ± 19 ps). The long-lived charge recombination process of *f*-TPE-PyH should be attributed to the fact that the distinctive TSC has stabilized the ICT state and slowed the charge recombination process.

For the purpose of further verifying that TSC has the positive effect on stabilizing the ICT state, *l*-TPE-Py, an isomer of *f*-TPE-Py with a linear configuration, is synthesized, and the corresponding protonated molecule *l*-TPE-PyH is also obtained (Figure S8). *l*-TPE-PyH has a prominent ICT effect, as proven by a solvatochromism experiment (Table S1). The
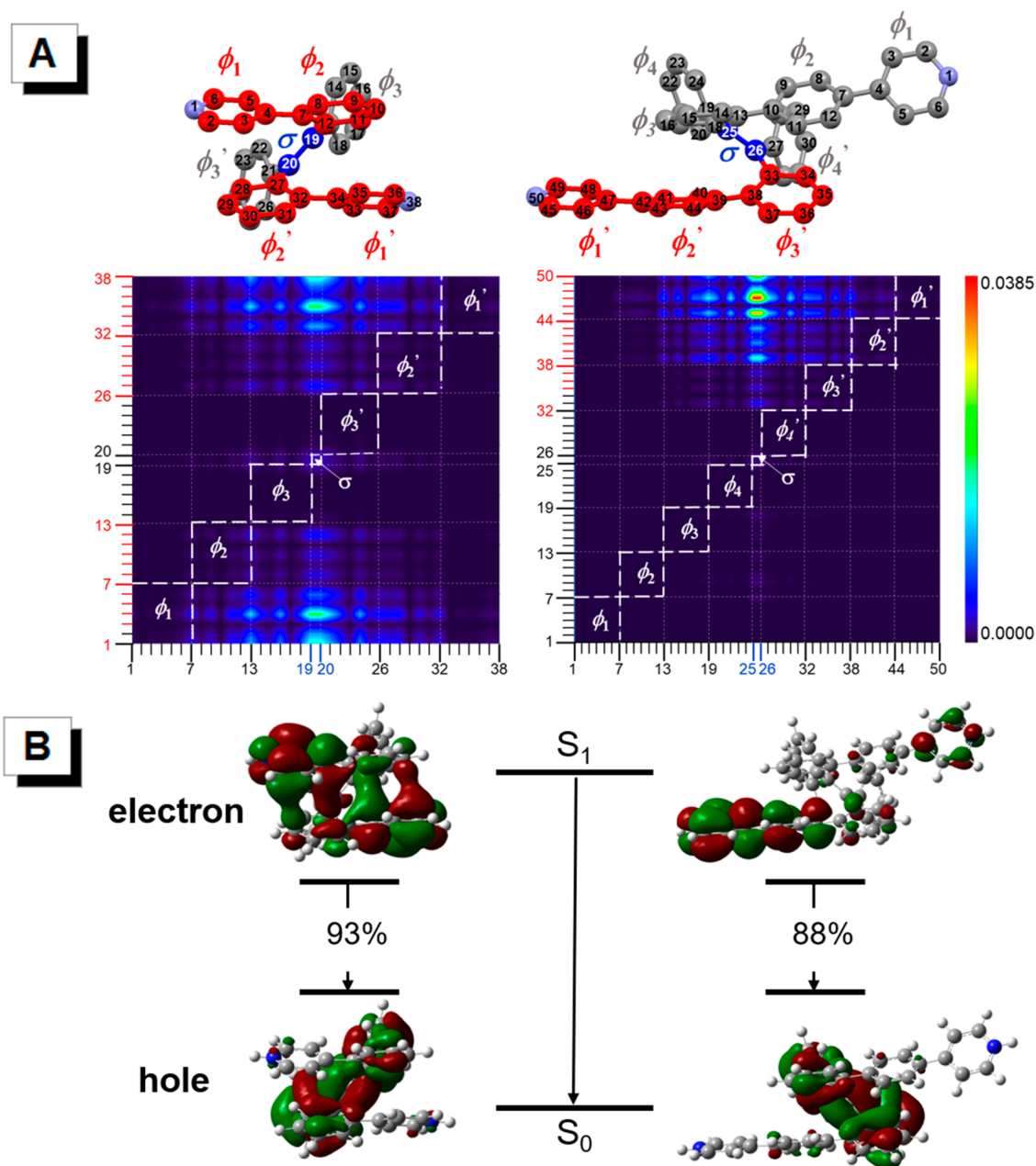
Figure 4. (A) Transition density matrixes and (B) natural transition orbitals of *f*-TPE-PyH (left) and *f*-TPE-PPyH (right).

fsTA spectra of *l*-TPE-PyH show that the original peak at 670 nm (at 0 ps) disappears within 1 ps. Meanwhile, new peaks at 570, 745, and 938 nm rise up as the peak at 670 nm decreases. All of these peaks decay thoroughly within 200 ps. There are 4 kinetic components found, and their lifetimes are estimated to be 0.9 ± 0.09, 1.9 ± 0.4, 8.1 ± 0.4, and 55 ± 3 ps, respectively. The kinetic component with the shortest lifetime of ~0.9 ps can be attributed to the internal conversion. The process with the lifetime of ~1.9 ps should be interpreted as the formation of the ICT state. The kinetic components with the lifetime of ~8.1 ps are due to the vibration relaxation process including the rotation of the aromatic rings.[46] Because of the flexible structure, the vibration relaxation process of *l*-TPE-PyH is faster than that of rigid foldamers. In addition, the charge recombination process (~55 ps) observed for *l*-TPE-PyH is about 10-fold quicker than those of the foldamers, because the

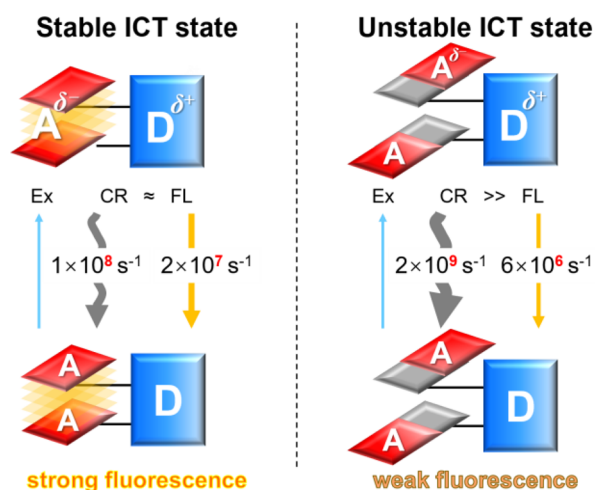better conjugation of the linear molecule endows it with stronger interactions between D and A.

The transition density matrix can provide information about the electron−hole localization and coherence of a specific excitation.[47,48] Therefore, it is helpful in visually analyzing the electronic excitation processes involving ICT. The numbers on the abscissa and ordinate represent numbers of non-hydrogen atoms. The hydrogen atoms are ignored by default because they usually have little contribution to the transition with which we are concerned. Colors represent the magnitude of the value to plot the transition density matrix: a large value in the diagonal term indicates the locally excited state of the corresponding atoms, while a large value in the nondiagonal term indicates the transition between two atoms. To gain deeper insights into the contributions of different moieties in $S_1 \rightarrow S_0$ transitions of *f*-TPE-PyH and *f*-TPE-PPyH, transition density matrixes are calculated by Multiwfn.[49] The atoms,

aromatic rings, and C=C double bonds in the foldamers are labeled for better understanding of the transition density matrix (Figure 4A). The holes of both foldamers are basically distributed at the central TPE moieties, but the electron distributions in the two foldamers are totally different. For *f*-TPE-PyH, both π-stacked phenylpyridine moieties contribute to the $S_1 \rightarrow S_0$ transition. The natural transition orbitals reveal that TSC helps to disperse the electrons on the two phenylpyridine moieties and within their interchain region in the excited state of *f*-TPE-PyH (Figure 4B). Such delocalized distribution can weaken D–A interaction in the excited state. Consequently, the charge recombination process is slowed down and the ICT state is stabilized. In sharp contrast, for *f*-TPE-PPyH, electrons are mainly distributed on one of the 4-(biphenyl-4-yl)pyridine moieties instead of the two 4-(biphenyl-4-yl)pyridine moieties or TPE moiety. In that case, the electron distribution in *f*-TPE-PPyH is much more concentrated, resulting in strong interaction. Hence, a nonradiative charge recombination process can occur readily in *f*-TPE-PPyH, causing weak fluorescence.

Scheme 2 illustrates the mechanism on how TSC stabilizes the ICT state. For the molecules without TSC, like *f*-TPE-

Scheme 2. Schematic Illustration of the Mechanism of TSC Stabilizing the ICT States[a]

[a]Ex, excitation; CR, charge recombination; FL, fluorescence.

PPyH, when they are excited to the ICT state, the charges are distributed in a concentrated pattern on D and A, leading to strong interactions between D and A. Therefore, the charge recombination process occurs at a great rate constant that can be 3–5 orders of magnitude larger than that of the fluoresce process. As a result, the ICT state is unstable and short-lived. In contrast, for the molecules with strong TSC character, like *f*-TPE-PyH, when they are excited to ICT states, the charges can be dispersed between the stacked aromatic rings, resulting in weak interactions between D and A. Therefore, these molecules have much longer ICT lifetimes. Because the nonradiative charge recombination process is slowed down, the k_{nr} is greatly decreased, which is beneficial to fluorescence. This is why *f*-TPE-PyH has much stronger fluorescence than *f*-TPE-PPyH.

In this work, we elucidate the interesting photophysical properties of pyridine-modified TPE-based foldamers *f*-TPE-Py and *f*-TPE-PPy and their protonated derivatives *f*-TPE-PyH

and *f*-TPE-PPyH. The unprotonated foldamers have TSC characters, which mainly contribute to the high-energy transition of $S_0 \rightarrow S_n$ but are of little avail for the fluorescence. Besides, they have negligible ICT effect and their fluorescence mainly originates from the TPE core. The protonated foldamers show remarkable ICT effect, but their TSC properties are totally different. *f*-TPE-PyH has a strong TSC, which plays a significant role in both absorption and fluorescence properties, while the TSC disappears in *f*-TPE-PPyH. As evidenced by the much longer lifetime, the ICT state in *f*-TPE-PyH is much more stable than that in *f*-TPE-PPyH. Owing to the strong TSC, the charges can be delocalized in the π-stacked region in *f*-TPE-PyH, leading to reduced interaction between D and A and thus a decreased nonradiative charge recombination rate. In consequence, *f*-TPE-PyH has a longer ICT lifetime and stronger fluorescence in comparison with other ICT molecules without TSC like *f*-TPE-PPyH. These results clearly demonstrate that TSC can efficiently stabilize the ICT state and could have a positive effect on the fluorescence of molecules with the ICT effect. The through-space conjugated foldamers with a stable ICT state could have a bright future in optoelectronics, photochemistry, and biotechnology.

■ ASSOCIATED CONTENT

Ⓢ Supporting Information

The Supporting Information is available free of charge on the ACS Publications website at DOI: 10.1021/acs.jpclett.9b01040.

Details of the chemicals, instrumentation, synthesis, characterization, and theoretical calculation; photophysical properties; calculated absorption UV−vis spectra and optimized geometries of *f*-TPE-PyH and *f*-TPE-PPyH in excited states; fsTA spectra of *l*-TPE-PyH (PDF)

■ AUTHOR INFORMATION

Corresponding Authors
*E-mail: mszjzhao@scut.edu.cn (Z.Z.).
*E-mail: tangbenz@ust.hk (B.Z.T.).

ORCID Ⓘ
Zujin Zhao: 0000-0002-0618-6024
Ben Zhong Tang: 0000-0002-0293-964X

Notes
The authors declare no competing financial interest.

■ REFERENCES

(1) Lee, J.; Ko, S.-J.; Seifrid, M.; Lee, H.; McDowell, C.; Luginbuhl, B. R.; Karki, A.; Cho, K.; Nguyen, T.-Q.; Bazan, G. C. Design of Nonfullerene Acceptors with Near-Infrared Light Absorption Capabilities. *Adv. Energy Mater.* **2018**, *8*, 1801209.

(2) Wei, Q.; Fei, N.; Islam, A.; Lei, T.; Hong, L.; Peng, R.; Fan, X.; Chen, L.; Gao, P.; Ge, Z. Small-Molecule Emitters with High Quantum Efficiency: Mechanisms, Structures, and Applications in OLED Devices. *Adv. Opt. Mater.* **2018**, *6*, 1800512.

(3) Chen, B.; Nie, H.; Hu, R.; Qin, A.; Zhao, Z.; Tang, B. Z. Red Fluorescent Siloles with Aggregation-Enhanced Emission Characteristics. *Sci. China: Chem.* 2016, 59, 699−706.

(4) Obondi, C. O.; Lim, G. N.; Jang, Y.; Patel, P.; Wilson, A. K.; Pod-Dutoori, P. K.; D'Souza, F. Charge Stabilization in High-Potential Zinc Porphyrin-Fullerene via Axial Ligation of Tetrathiafulvalene. *J. Phys. Chem. C* 2018, 122, 13636−13647.

(5) Sampaio, R. N.; Troian-Gautier, L.; Meyer, G. J. A Charge-Separated State that Lives for Almost a Second at a Conductive Metal Oxide Interface. *Angew. Chem., Int. Ed.* 2018, 57, 15390−15394.

(6) Wang, T.; Weerasinghe, K. C.; Sun, H.; Hu, X.; Lu, T.; Liu, D.; Hu, W.; Li, W.; Zhou, X.; Wang, L. Effect of Triplet State on the Lifetime of Charge Separation in Ambipolar D-A$_1$-A$_2$ Organic Semiconductors. *J. Phys. Chem. C* 2016, 120, 11338−11349.

(7) Xu, B.; Wang, C.; Ma, W.; Liu, L.; Xie, Z.; Ma, Y. Photoinduced Electron Transfer in Asymmetrical Perylene Diimide: Understanding the Photophysical Processes of Light-Absorbing Nonfullerene Acceptors. *J. Phys. Chem. C* 2017, 121, 5498−5502.

(8) Xu, M.; Li, R.; Pootrakulchote, N.; Shi, D.; Guo, J.; Yi, Z.; Zakeeruddin, S. M.; Grätzel, M.; Wang, P. Energy-Level and Molecular Engineering of Organic D-π-A Sensitizers in Dye-Sensitized Solar Cells. *J. Phys. Chem. C* 2008, 112, 19770−19776.

(9) Song, J.; Zhang, F.; Li, C.; Liu, W.; Li, B.; Huang, Y.; Bo, Z. Phenylethyne-Bridged Dyes for Dye-Sensitized Solar Cells. *J. Phys. Chem. C* 2009, 113, 13391−13397.

(10) Wheeler, S. E. Understanding Substituent Effects in Non-covalent Interactions Involving Aromatic Rings. *Acc. Chem. Res.* 2013, 46, 1029−1038.

(11) Grimme, S. Do Special Noncovalent π−π Stacking Interactions Really Exist? *Angew. Chem., Int. Ed.* 2008, 47, 3430−3434.

(12) Zafra, J. L.; Ontoria, A. M.; Mayorga Burrezo, P.; Peña-Alvarez, M.; Samoc, M.; Szeremeta, J.; Ramírez, F. J.; Lovander, M. D.; Droske, C. J.; Pappenfus, T. M.; Echegoyen, L.; Navarrete, J. T. L.; Martín, N.; Casado, J. Fingerprints of Through-Bond and Through-Space Exciton and Charge π-Electron Delocalization in Linearly Extended [2.2]Paracyclophanes. *J. Am. Chem. Soc.* 2017, 139, 3095−3105.

(13) Morisaki, Y.; Kawakami, N.; Shibata, S.; Chujo, Y. Through-Space Conjugated Molecular Wire Comprising Three π-Electron Systems. *Chem. - Asian J.* 2014, 9, 2891−2895.

(14) Hasegawa, M.; Kobayakawa, K.; Matsuzawa, H.; Nishinaga, T.; Hirose, T.; Sako, K.; Mazaki, Y. Macrocyclic Oligothiophene with Stereogenic [2.2]Paracyclophane Scaffolds: Chiroptical Properties from π-Transannular Interactions. *Chem. - Eur. J.* 2017, 23, 3267−3271.

(15) Gon, M.; Morisaki, Y.; Chujo, Y. Optically Active Phenylethene Dimers Based on Planar Chiral Tetrasubstituted [2.2]Paracyclophane. *Chem. - Eur. J.* 2017, 23, 6323−6329.

(16) Spuling, E.; Sharma, N.; Samuel, I. D. W.; Zysman-Colman, E.; Brase, S. (Deep) Blue Through-Space Conjugated TADF Emitters Based on [2.2]Paracyclophanes. *Chem. Commun.* 2018, 54, 9278−9281.

(17) Hirose, T.; Tsunoi, Y.; Fujimori, Y.; Matsuda, K. Fluorescence Enhancement of Covalently Linked 1-Cyano-1,2-diphenylethene Chromophores with Naphthalene-1,8-diyl Linker Units: Analysis Based on Kinetic Constants. *Chem. - Eur. J.* 2015, 21, 1637−1644.

(18) Schmidt, H. C.; Spulber, M.; Neuburger, M.; Palivan, C. G.; Meuwly, M.; Wenger, O. S. Charge Transfer Pathways in Three Isomers of Naphthalene-Bridged Organic Mixed Valence Compounds. *J. Org. Chem.* 2016, 81, 595−602.

(19) Sinnwell, M. A.; MacGillivray, L. R. Halogen-Bond-Templated [2 + 2] Photodimerization in the Solid State: Directed Synthesis and Rare Self-Inclusion of a Halogenated Product. *Angew. Chem., Int. Ed.* 2016, 55, 3477−3480.

(20) Rios, C.; Salcedo, R. Computational Study of Electron Delocalization in Hexaarylbenzenes. *Molecules* 2014, 19, 3274−3296.

(21) Vij, V.; Bhalla, V.; Kumar, M. Hexaarylbenzene: Evolution of Properties and Applications of Multitalented Scaffold. *Chem. Rev.* 2016, 116, 9565−9627.

(22) Zhen, S.; Mao, J. C.; Chen, L.; Ding, S.; Luo, W.; Zhou, X. S.; Qin, A.; Zhao, Z.; Tang, B. Z. Remarkable Multichannel Conductance of Novel Single-Molecule Wires Built on Through-Space Conjugated Hexaphenylbenzene. *Nano Lett.* 2018, 18, 4200−4205.

(23) Morisaki, Y.; Sawamura, T.; Murakami, T.; Chujo, Y. Synthesis of Anthracene-Stacked Oligomers and Polymer. *Org. Lett.* 2010, 12, 3188−3191.

(24) Hayashi, S.; Yamamoto, S.-i.; Koizumi, T. A Cyclic Compound based on Xanthene-Linked π-Stacked Dimer via Direct Arylation. *Chem. Lett.* 2017, 46, 200−203.

(25) Vemuri, G. N.; Pandian, R. R.; Spinello, B. J.; Stopler, E. B.; Kinney, Z. J.; Hartley, C. S. Twist Sense Control in Terminally Functionalized ortho-Phenylenes. *Chem. Sci.* 2018, 9, 8260−8270.

(26) Hartley, C. S. Folding of *ortho*-Phenylenes. *Acc. Chem. Res.* 2016, 49, 646−654.

(27) Mathew, S.; Crandall, L. A.; Ziegler, C. J.; Hartley, C. S. Enhanced Helical Folding of *ortho*-Phenylenes through the Control of Aromatic Stacking Interactions. *J. Am. Chem. Soc.* 2014, 136, 16666−16675.

(28) Yamauchi, Y.; Yoshizawa, M.; Akita, M.; Fujita, M. Engineering Double to Quintuple Stacks of a Polarized Aromatic in Confined Cavities. *J. Am. Chem. Soc.* 2010, 132, 960−966.

(29) Kiguchi, M.; Kaneko, S. Electron Transport through Single π-Conjugated Molecules Bridging between Metal Electrodes. *ChemPhysChem* 2012, 13, 1116−1126.

(30) Hua, C.; Doheny, P. W.; Ding, B.; Chan, B.; Yu, M.; Kepert, C. J.; D'Alessandro, D. M. Through-Space Intervalence Charge Transfer as a Mechanism for Charge Delocalization in Metal−Organic Frameworks. *J. Am. Chem. Soc.* 2018, 140, 6622−6630.

(31) Kaufmann, C.; Bialas, D.; Stolte, M.; Wurthner, F. Discrete π-Stacks of Perylene Bisimide Dyes within Folda-Dimers: Insight into Long- and Short-Range Exciton Coupling. *J. Am. Chem. Soc.* 2018, 140, 9986−9995.

(32) Winterfeld, K. A.; Lavarda, G.; Guilleme, J.; Sekita, M.; Guldi, D. M.; Torres, T.; Bottari, G. ubphthalocyanines Axially Substituted with a Tetracyanobuta-1,3-diene−Aniline Moiety: Synthesis, Structure, and Physicochemical Properties. *J. Am. Chem. Soc.* 2017, 139, 5520−5529.

(33) Shen, P.; Zhuang, Z.; Zhao, Z.; Tang, B. Z. Recent Advances of Folded Tetraphenylethene Derivatives Featuring Through-Space Conjugation. *Chin. Chem. Lett.* 2016, 27, 1115−1123.

(34) Zhuang, Z.; Shen, P.; Ding, S.; Luo, W.; He, B.; Nie, H.; Wang, B.; Huang, T.; Hu, R.; Qin, A.; Zhao, Z.; Tang, B. Z. Synthesis, Aggregation-Enhanced Emission, Polymorphism and Piezochromism of TPE-Cored Foldamers with Through-Space Conjugation. *Chem. Commun.* 2016, 52, 10842−10745.

(35) He, B.; Luo, W.; Hu, S.; Chen, B.; Zhen, S.; Nie, H.; Zhao, Z.; Tang, B. Z. Synthesis and Photophysical Properties of New Through-Space Conjugated Luminogens Constructed by Folded Tetraphenylethene. *J. Mater. Chem. C* 2017, 5, 12553−12560.

(36) Zhao, Z.; Lam, J. W.; Chan, C. Y.; Chen, S.; Liu, J.; Lu, P.; Rodriguez, M.; Maldonado, J. L.; Ramos-Ortiz, G.; Sung, H. H.; Williams, I. D.; Su, H.; Wong, K. S.; Ma, Y.; Kwok, H. S.; Qiu, H.; Tang, B. Z. Stereoselective Synthesis, Efficient Light Emission, and High Bipolar Charge Mobility of Chiasmatic Luminogens. *Adv. Mater.* 2011, 23, 5430−5435.

(37) Chen, L.; Wang, Y.-H.; He, B.; Nie, H.; Hu, R.; Huang, F.; Qin, A.; Zhou, X.-S.; Zhao, Z.; Tang, B. Z. Multichannel Conductance of Folded Single-Molecule Wires Aided by Through-Space Conjugation. *Angew. Chem., Int. Ed.* 2015, 54, 4231−4235.

(38) He, B.; Nie, H.; Chen, L.; Lou, X.; Hu, R.; Qin, A.; Zhao, Z.; Tang, B. Z. High Fluorescence Efficiencies and Large Stokes Shifts of Folded Fluorophores Consisting of a Pair of Alkenyl-Tethered, π-Stacked Oligo-*p*-phenylenes. *Org. Lett.* 2015, 17, 6174−6177.

(39) Luo, W.; Nie, H.; He, B.; Zhao, Z.; Peng, Q.; Tang, B. Z. Spectroscopic and Theoretical Characterization of Through-Space Conjugation of Foldamers with A Tetraphenylethene Hinge. *Chem. - Eur. J.* 2017, 23, 18041−18048.

(40) Zhao, Z.; He, B.; Nie, H.; Chen, B.; Lu, P.; Qin, A.; Tang, B. Z. Stereoselective Synthesis of Folded Luminogens with Arene-Arene Stacking Interactions and Aggregation-Enhanced Emission. *Chem. Commun.* **2014**, *50*, 1131−1133.

(41) He, R.; Yuan, Y.; Shen, W.; Li, M.; Yao, L. Quantum Chemical Study on Excited States and Charge Transfer of Oxazolo[4,5-B]Pyridine Derivatives. *Sci. China: Chem.* **2012**, *55*, 2186−2196.

(42) Moreno Oliva, M.; Casado, J.; Navarrete, J. T. L.; Hennrich, G.; Delgado, M. C. R.; Orduna, J. Linear and Nonlinear Optical Properties of Pyridine-Based Octopolar Chromophores Designed for Chemical Sensing. Joint Spectroscopic and Theoretical Study. *J. Phys. Chem. C* **2007**, *111*, 18778−18784.

(43) Valeur, B. *Molecular Fluorescence: Principles and Application*; Wiley-VCH: Weinheim, 2002; p 211.

(44) Li, W.; Liu, D.; Shen, F.; Ma, D.; Wang, Z.; Feng, T.; Xu, Y.; Yang, B.; Ma, Y. A Twisting Donor-Acceptor Molecule with an Intercrossed Excited State for Highly Efficient, Deep-Blue Electroluminescence. *Adv. Funct. Mater.* **2012**, *22*, 2797−2803.

(45) Choi, J.; Ahn, D. S.; Oang, K. Y.; Cho, D. W.; Ihee, H. Charge Transfer-Induced Torsional Dynamics in the Excited State of 2,6-Bis(diphenylamino)anthraquinone. *J. Phys. Chem. C* **2017**, *121*, 24317−24323.

(46) Cai, Y.; Du, L.; Samedov, K.; Gu, X.; Qi, F.; Sung, H. H. Y.; Patrick, B. O.; Yan, Z.; Jiang, X.; Zhang, H.; Lam, J. W. Y.; Williams, I. D.; Phillips, D. L.; Qin, A.; Tang, B. Z. Deciphering the Working Mechanism of Aggregation-Induced Emission of Tetraphenylethylene Derivatives by Ultrafast Spectroscopy. *Chem. Sci.* **2018**, *9*, 4662−4670.

(47) Biswas, S.; Pramanik, A.; Pal, S.; Sarkar, P. A Theoretical Perspective on the Photovoltaic Performance of S,N-Heteroacenes: An Even-Odd Effect on the Charge Separation Dynamics. *J. Phys. Chem. C* **2017**, *121*, 2574−2587.

(48) Sui, M.; Li, S.; Pan, Q.; Sun, G.; Geng, Y. Theoretical Characterization on Photoelectric Properties of Benzothiadiazole- and Fluorene-Based Small Molecule Acceptor Materials for the Organic Photovoltaics. *J. Mol. Model.* **2017**, *23*, 28.

(49) Lu, T.; Chen, F. J. Multiwfn: A Multifunctional Wavefunction Analyzer. *J. Comput. Chem.* **2012**, *33*, 580−592.